Biomechanical analyses of pterygotid sea scorpion chelicerae uncover predatory specialisation within eurypterids

Russell D C Bicknell [Corresp., 1, 2] , **Yuri Simone** [3] , **Arie van der Meijden** [3] , **Stephen Wroe** [1, 2] , **Greg Edgecombe** [4] , **John R Paterson** [1]

[1] Palaeoscience Research Centre, School of Environmental & Rural Science, University of New England, Armidale, NSW, Australia

[2] Function, Evolution and Anatomy Research Lab, School of Environmental and Rural Science, University of New England, Armidale, NSW, Australia

[3] CIBIO Research Centre in Biodiversity and Genetic Resources, Vila do Conde, Portugal

[4] Department of Earth Sciences, The Natural History Museum, London, UK

Corresponding Author: Russell D C Bicknell
Email address: rdcbicknell@gmail.com

Eurypterids (sea scorpions) are extinct aquatic chelicerates. Within this group, members of Pterygotidae represent some of the largest known marine arthropods. Representatives of this family all have hypertrophied, anteriorly-directed chelicerae and are commonly considered Silurian and Devonian apex predators. Despite a long history of research interest in these appendages, pterygotids have been subject to limited biomechanical investigation. Here we present finite element analysis (FEA) models of four different pterygotid chelicerae—those of *Acutiramus bohemicus*, *Erettopterus bilobus*, *Jaekelopterus rhenaniae*, and *Pterygotus anglicus*—informed through muscle data and finite element models (FEM) of chelae from 16 extant scorpion taxa. We find that *Er. bilobus* and *Pt. anglicus* have comparable stress patterns to modern scorpions, suggesting a generalised diet that probably included other eurypterids and, in the Devonian species, armoured fishes, as indicated by co-occurring fauna. *Acutiramus bohemicus* is markedly different, the stress being concentrated in the proximal fixed ramus rather than the serrated denticles. This stress, focused into one region, indicates a morphology better suited for targeting softer prey. *Jaekelopterus rhenaniae* exhibits much lower stress across the entire model. This, combined with an extremely large body size, suggests that this species likely preyed on larger and harder prey, including heavily armoured fishes. The range of cheliceral morphologies and stress patterns within Pterygotidae demonstrate that members of this family had variable diets, with only the most derived species likely to feed on armoured prey, such as placoderms. Indeed, increased sizes of these forms throughout the mid-Palaeozoic may represent an 'arms race' between eurypterids and armoured fishes, with Devonian pterygotids adapting to the rapid diversification of placoderms.

1 **Biomechanical analyses of pterygotid sea scorpion chelicerae uncover predatory**

2 **specialisation within eurypterids**

3 Russell D. C. Bicknell[1,2,*], Yuri Simone[3], Arie van der Meijden[3], Stephen Wroe[1,2], Gregory D.

4 Edgecombe[4], and John R. Paterson[1]

5 [1] Palaeoscience Research Centre, School of Environmental & Rural Science, University of New

6 England, Armidale, NSW 2351, Australia

7 [2] Function, Evolution and Anatomy Research Lab, School of Environmental and Rural Science,

8 University of New England, Armidale, NSW 2351, Australia

9 [3]CIBIO Research Centre in Biodiversity and Genetic Resources, InBIO, Universidade do Porto,

10 Campus Agrário de Vairão, Rua Padre Armando Quintas 7, 4485–661 Vairão, Vila do Conde,

11 Portugal

12 [4] Department of Earth Sciences, The Natural History Museum, London SW7 5BD, UK

13 [*] corresponding author: rbickne2@une.edu.au

16 **Abstract**

17 Eurypterids (sea scorpions) are extinct aquatic chelicerates. Within this group, members of

18 Pterygotidae represent some of the largest known marine arthropods. Representatives of this

19 family all have hypertrophied, anteriorly-directed chelicerae and are commonly considered

20 Silurian and Devonian apex predators. Despite a long history of research interest in these

21 appendages, pterygotids have been subject to limited biomechanical investigation. Here we

22 present finite element analysis (FEA) models of four different pterygotid chelicerae—those of

23 *Acutiramus bohemicus*, *Erettopterus bilobus*, *Jaekelopterus rhenaniae*, and *Pterygotus*

24 *anglicus*—informed through muscle data and finite element models (FEM) of chelae from 16

25 extant scorpion taxa. We find that *Er. bilobus* and *Pt. anglicus* have comparable stress patterns to

26 modern scorpions, suggesting a generalised diet that probably included other eurypterids and, in

27 the Devonian species, armoured fishes, as indicated by co-occurring fauna. *Acutiramus*

28 *bohemicus* is markedly different, the stress being concentrated in the proximal fixed ramus rather

29 than the serrated denticles. This stress, focused into one region, indicates a morphology better

30 suited for targeting softer prey. *Jaekelopterus rhenaniae* exhibits much lower stress across the

31 entire model. This, combined with an extremely large body size, suggests that this species likely

32 preyed on larger and harder prey, including heavily armoured fishes. The range of cheliceral

33 morphologies and stress patterns within Pterygotidae demonstrate that members of this family

34 had variable diets, with only the most derived species likely to feed on armoured prey, such as

35 placoderms. Indeed, increased sizes of these forms throughout the mid-Palaeozoic may represent

36 an 'arms race' between eurypterids and armoured fishes, with Devonian pterygotids adapting to

37 the rapid diversification of placoderms.

38 **Keywords:** Euarthropoda, finite element analysis, predation, eurypterids, sea scorpions

39 **Introduction**

40   Feeding toolkits of proposed fossil predators are typically explored through functional

41   morphology, often with comparison to modern analogues. In the last two decades, there has been

42   a focus on modelling animals using two-dimensional (2D) and three-dimensional (3D)

43   biomechanical analyses, including finite element analyses (FEA) (Ross, 2005; Rayfield, 2007;

44   van Heteren et al., 2021; Rowe & Snively, 2022). This latter method has been an effective

45   approach for modelling fossil vertebrates and, as such, applications of FEA in palaeontology

46   have largely focused on select vertebrate groups (Rayfield et al., 2001; Wroe et al., 2005, 2007,

47   2018; Kupczik et al., 2009; Strait et al., 2009; Attard et al., 2016). By comparison, fossil

48   arthropods have not been examined as thoroughly with 3D FEA (Bicknell et al., 2018a, 2021;

49   Esteve et al., 2021). Recent focus on modelling extinct arthropods has increased knowledge of

50   the biomechanical capability of these fossil forms.

51   Fossil predatory arthropods are epitomised by the large, aquatic eurypterid family,

52   Pterygotidae, known from Silurian and Lower Devonian deposits (Braddy et al., 2008; McCoy et

53   al., 2015; Lamsdell & Selden, 2017). Some forms have bodies reaching ~2.5 m in length and

54   represent the largest known marine arthropods, living or extinct (Braddy et al., 2008; Lamsdell &

55   Braddy, 2010; Vermeij, 2016). A key feature of pterygotids is their large, anteriorly-directed

56   chelicerae that often show enlarged denticles (Ciurca & Tetlie, 2007), likely used to capture and

57   subdue prey (Kjellesvig-Waering, 1964; Waterston, 1964; Miller, 2007b; Braddy et al., 2008;

58   Kennedy et al., 2012; Bicknell et al., 2020). Given this, pterygotids are presumed to have been

59   apex predators within their respective ecosystems (Selden, 1984; Plotnick & Baumiller, 1988;

60   Braddy et al., 2008). Despite the striking appearance of pterygotid chelicerae, to date,

61   biomechanical investigations of these structures have been limited to 2D lever arm studies

62   (Selden, 1984; Laub et al., 2010). Examination of these chelicerae using 3D biomechanical

63   analysis could therefore present a more complete understanding of their functional morphology.

64   Importantly, modern scorpion pedipalp chelae can inform on the mechanical performance of

65   pterygotid chelicerae, as the former are perhaps the closest functional analogue for the fossil

66   forms. Furthermore, as scorpions are a diverse chelicerate group that are phylogenetically closer

67   to eurypterids than other arthropod groups with chelate appendages such as decapod crustaceans

68   (Shultz, 2007; Legg et al., 2013; Haug, 2020), and likely have comparable cuticular properties to

69   eurypterids, scorpions are one of the more informative groups to function as modern analogues.

70   Pterygotid chelicerae occasionally preserve with sufficient anatomical fidelity to allow

71   for detailed reconstructions. In particular, *Acutiramus bohemicus*, *Erettopterus bilobus*,

72   *Jaekelopterus rhenaniae*, and *Pterygotus anglicus* are four exceptionally preserved and well

73   documented species, making them ideal for biomechanical analysis (Waterston, 1964; Chlupáč,

74   1994; Poschmann & Tetlie, 2006; Miller, 2007b; Braddy et al., 2008; Dunlop et al., 2020).

75   Furthermore, modern scorpions provide a diverse and well-studied group for comparative

76   purposes (Van der Meijden et al., 2012a; Lourenço, 2021). Building on previous FEAs of

77   scorpions (Van der Meijden et al., 2012a) and analyses of extinct arthropods (Bicknell et al.,

78   2021), here we present 3D finite element models (FEMs) of the chelicerae of *Ac. bohemicus*, *Er.*

79   *bilobus*, *Ja. rhenaniae*, and *Pt. anglicus* and compare them to models of chelae of 16 scorpion

80   taxa.

81   **Methods**

82   *Extant models*

83   Information on the muscle that adducts the moveable finger in a scorpion chela follows

84   Snodgrass (1952), Gilai & Parnas (1970), and Van der Meijden et al. (2012a) (Figure 1A). One

85   primary muscle mass fills the majority of the proximal manus region and is responsible for

86   adducting the moveable finger. There is also a secondary closing muscle in the patella (Gilai &

87   Parnas, 1970). We have not considered this muscle here because: (a) scans of patellar sections

88   needed to estimate muscle size were not made; and (b) there is no fossil evidence for this muscle

89   (such as scars or fibres) in eurypterids. Data for calculating force of the primary closing muscle

90   were collected from micro computed tomography (micro-CT) scans. The scans were made with a

91   Skyscan 1076 micro-CT scanner using a source voltage of 31 kV and a source current of 187 µA

92   at 35 µm resolution, as detailed in Van der Meijden et al. (2012a). Sixteen specimens, each

93   representing a different scorpion genus and spanning six families, were scanned and chelae

94   segmented with Amira/Avizo 5 (Thermo Fischer Scientific). The external chela cuticle and

95   internal manus content were segmented either manually or using the "Thresholding" tool in

96   Amira. Internal manus content, excluding regions where adducting muscles were not present,

97   was segmented as a globular structure to estimate muscle volume, surface area, and cross-

98   sectional area. Values of volume and area were calculated with the "Surface Area Volume"

99   module in Avizo, while the cross-sectional area was calculated by bisecting the muscle volume

100   transversely (i.e. perpendicular to the proximal-distal axis of the manus and approximately

101   perpendicular to muscle fibre directions) in Meshlab v. 2020.12 (Cignoni et al., 2008). Analysed

102   specimens are preserved in ethanol and housed in the Centro de Investigação em Biodiversidade

103   e Recursos Genéticos, Vila do Conde, Portugal (CIBIO) collection and assigned the prefix of

104   'Sc'.

105   Maximum pinch force data were only known from the micro-CT scanned specimens of

106 *Androctonus bicolor* and *Pandinoides cavimanus* (Simone & Van der Meijden, 2018). As we did

107 not measure in-vivo pinch forces of the micro-CT scanned individuals of other species, pinch

108 forces were estimated for those specimens using data available from other individuals of the

109 same species. As such, chela length, height, and width (Stahnke, 1970) were used to predict

110 pinch force for our FEMs based on known pinch forces of other individuals of the same species

111 (Van der Meijden et al., 2010, 2012a; Supplemental Table 1). The data were $\log_{10}$ transformed to

112 linearise variables with different dimensionality and used to produced species-specific linear

113 models, and associated regression coefficients (Supplemental Table 2).

114   The mechanical advantage of the moveable finger was calculated from the micro-CT

115 scans following Simone & Van der Meijden (2018). However, as in-vivo pinch forces were

116 measured approximately two thirds of the finger length from the joint and not the distal-most

117 point of movable fingers, the mechanical advantage was corrected by shortening the length of the

118 out-lever by one third. Muscle force at insertion was then calculated for scanned specimens by

119 dividing pinch force by the specimens' mechanical advantage (Supplemental Table 3). Muscle

120 stresses used here were derived from Van der Meijden et al. (2012b), where the stress of

121 *Galeodes* sp. (203 kPa) and *Rhagodes* sp. (905 kPa) were employed as upper and lower bounds,

122 respectively (Supplementary Table 4). The manus and movable finger reconstructions were

123 exported from Amira as .STL files for analysis. The manus and moveable finger sections for

124 assessed specimens were then imported into 3-matic version 12 (Materialise, Leuven, Belgium)

125 and solid-meshed as distinct solid homogeneous structures consisting of tet-4 elements and the

126 gape angle was set to biologically realistic values between 10–30º. These models were then

127 exported as Nastran files for import into Strand7 (Strand7 Pty Ltd, NSW, Sydney, Australia)

128 FEA software. Material properties used are a Young's modulus of 7 GPa and a Poisson's ratio of

129 0.3—values used for scorpion cuticle following Van der Meijden et al. (2012a). Muscle origins

130 were tessellated as beam elements onto the Nastran models (Bicknell et al., 2018b). This was

131 done following successful applications to other arthropods (Bicknell et al., 2018b, 2021) and

132 allowed for a large muscle origin area to be modelled. Muscle forces (Supplemental Table 3)

133 were assigned to trusses directed toward the insertion site – the most proximal section of the

134 moveable finger. These insertions were treated as static points at the beam terminus. Three

135 denticles along both the manus and moveable finger were constrained in all directions at their

136 most apical node (Figure 1A); selected denticles were located at the proximal, mid-length, and

137 distal regions of the manus and finger. A hinge between the manus and moveable finger was

138 constructed using two sections: one link on either side of the proximoventral section of the

139 moveable finger. This emulates a simplified action of manus and moveable finger closure. A

140 colour-coded von Mises (VM) stress map was generated after solving models. Loaded Strand7

141 models are presented as Supplemental Data 1–16. These data are found at

142 10.17605/OSF.IO/GV8J5 Additionally, the analysed .STL files were used to generate 3D PDFs

143 using Tetra4D (Adobe Systems). Scorpion 3D PDFs are available from

144 10.17605/OSF.IO/GV8J5.

145   *Fossil models*

146 3D reconstructions of the *Acutiramus bohemicus*, *Erettopterus bilobus*, *Jaekelopterus rhenaniae*,

147 and *Pterygotus anglicus* chelicerae (fixed and free rami) were rendered in Zbrush (Pixologic,

148 Inc). Reconstructions were informed by examining selected fossils and published high resolution

149 images of chelicerae (Størmer, 1936; Waterston, 1964; Selden, 1984; Chlupáč, 1994; Poschmann

150 & Franke, 2006; Poschmann & Tetlie, 2006; Miller, 2007a, b; Braddy et al., 2008; Lomax et al.,

151   2011; Kennedy et al., 2012; Supplemental Table 4). These specimens permitted the modelling of

152   chelicerae with anatomically correct dimensions in lateral view. Considering the modern

153   analogues and the 2D preservation of the fossil forms, the degree of cheliceral 'inflation' was

154   informed through examining the three-dimensionality of the modelled scorpion chelae.

155   Furthermore, as there is no evidence to suggest that the fixed ramus is more inflated than the

156   movable ramus, both pterygotid rami were modelled with a similar degree of inflation. The

157   models were built with internal cavities informed by the scorpion scans and internal cavities of

158   fixed and free rami do not extend into the denticles, following the observations of modern

159   scorpions (Van der Meijden et al., 2012a; Kellersztein et al., 2019). These reconstructions were

160   required as the examined chelicerae are preserved as compression fossils, with very little relief.

161   There is little to no density difference between the fossil and the host matrix, and scanning these

162   fossils would have produced unreliable 3D data. Furthermore, if the scans were successful, the

163   models would have been retro-deformed, likely using scorpions as the reference. The

164   reconstructions presented here circumvent this limitation of the fossil record. Reconstructions

165   were exported as .STL files from Zbrush. These can be found in Supplemental Data 17–20,

166   available from 10.17605/OSF.IO/GV8J5.

167   The .STL files were scaled to the size of the largest known chelicerae of the respective

168   species to allow for a comparison between presumed adult forms (Waterston, 1964; Chlupáč,

169   1994; Miller, 2007b; Braddy et al., 2008). This scaling also allowed the calculation of muscle

170   force values for adult pterygotids and permitted the modelling of appendages at 'life size' scales.

171   We did not scale the pterygotid models to the size of scorpion chelae (Dumont et al., 2009;

172   Bicknell et al., 2021) as there are orders of magnitude difference in size between scorpion chelae

173   and pterygotid chelicerae. Scaling down chelicerae would likely have introduced allometric

174   errors to the modelling, increasing the uncertainty associated with the pterygotid models. Also,

175   deciding on a particular size to scale the specimens down to is highly subjective. Finally, we

176   were interested in examining the absolute size of chelicerae in particular in this study, thus

177   scaling to the volume of a scorpion chela would have not permitted this approach.

178   After scaling to life size, the .STL files of fixed and free rami were loaded into Meshlab

179   version 2020.12 to estimate the internal volume of the fixed ramus; a proxy for muscle force at

180   the insertion. The internal volume was calculated with the "Ambient Occlusion" filter in

181   Meshlab. All non-occluded elements and the fixed ramus finger were removed to produce the

182   proximal fixed ramus internal morphology. A convex hull of this morphology was then produced

183   and used to calculate the volume and surface area of the internal proximal fixed ramus–a proxy

184   for the size of the adducting muscle. The transverse section of this convex hull representing the

185   muscle mass was used as an estimate of muscle cross-sectional area. These data were $\log_{10}$

186   transformed and input into the scorpion muscle force regression model to calculate pterygotid

187   muscle force (Supplemental Table 5).

188   Force at the muscle insertion for pterygotid species was estimated using data from extant

189   scorpions by two methods: 1) extrapolation of a linear model; and 2) using muscle stress and

190   estimated pterygotid muscle cross sectional area. We only used the force estimates from the first

191   approach in the FEA models of the pterygotids, as this approach has the fewest assumptions.

192   However, we report and discuss both methods here, as the differences in estimated muscle force

193   obtained may be a cautionary example for other workers using only a single method to estimate

194   muscle force.

195   In the first approach, all calculated forces at muscle insertions, derived from in-vivo

196   pinch force measurements of the scorpions, were used to create a linear model to predict

197   pterygotid muscle force (Supplemental Tables 6, 7). The forces at muscle insertions were

198   considered dependent variables against the independent variables of muscle surface and volume.

199   Data were linearized by $\log_{10}$ transformation before running the model. The regression

200   coefficients were then used to estimate pterygotid input force at muscle insertions. All the

201   statistical regressions were performed in R version 4.1.2 (R Development Core Team, 2021;

202   Supplemental Code 1). Estimated muscle forces employed in the FEMs are shown in

203   Supplemental Table 3. In the second approach, estimates of muscle stress from Van der Meijden

204   et al. (2012b) were used to calculate pterygotid muscle force by multiplying these values with

205   pterygotid muscle cross-sectional area.

206   Boundary, loading, and restraining conditions applied to the cheliceral reconstructions

207   (Figure 1) were comparable to the scorpion models. Material properties used were the same as

208   scorpions, as the cuticle properties of pterygotid chelicerae are unknown. Muscle origin location,

209   size, and vectors were estimated based on the scorpion comparisons. Muscle origins are located

210   in the fixed ramus proximal region. Similar to scorpion models, muscle origins were tessellated

211   as beam elements. Muscle forces (Supplemental Table 8) were assigned to trusses directed

212   toward the insertion, in the proximal free ramus section, following Braddy et al. (2008). Similar

213   to scorpion models, three denticles on the fixed and movable rami were constrained. However, as

214   pterygotid denticles vary in size, the largest denticles were constrained because these points

215   would be the first regions to have contacted prey (Figure 1B). A colour-coded VM brick stress

216   map was generated after solving models. The loaded Stand7 models are presented in

217   Supplemental Data 17–20, available from 10.17605/OSF.IO/GV8J5.

218   As the pterygotid chelicerae cannot be scanned, there is uncertainty regarding the thickness

219   of the ramus cuticle. Although eurypterid cuticle from the carapace and gnathobases has been

220   sectioned in previous studies (Dalingwater, 1973, 1975, 1985; Bicknell et al., 2018b), there is no

221   published information on the cuticle thickness of pterygotid chelicerae. Therefore, sensitivity

222   tests for pterygotid models were conducted to explore the impact of cuticle thickness on the

223   biomechanical modelling. *Erettopterus bilobus* fixed and free rami were reconstructed with

224   thinner and thicker cuticle relative to the presented model. Further, this taxon was reconstructed

225   and analysed with cuticle extending into the constrained denticles. These sensitivity test models

226   (loading and boundary conditions outlined below) showed very comparable stress distributions

227   (Supplemental Figure 1; Supplemental Data 17). This suggests that hollowing the rami and

228   denticles has limited impact on the VM stress distribution, but does influence the stress

229   magnitudes.

230   Since pterygotid material properties are unknown, it is possible that the values used here may

231   have influenced the VM stresses estimated from the FEMs. Consequently, our results should be

232   considered in comparative contexts only. We therefore limit our interpretation of the models to

233   stress distributions rather than magnitudes, as the former is less sensitive to variation in the

234   assumptions included in our models, such as muscle force, cuticle thickness and material

235   properties.

236   Mean VM stress values were calculated from all FEM models in Strand7. These values were

237   plotted against the volume of chelae and chelicerae models, exported from Geomagic Studio (3D

238   Systems, North Carolina, USA). Both values were $\log_{10}$ transformed (Supplemental Table 9) and

239   plotted in bivariate space.

240   **Results**

241   The linear model used to estimate muscle force for the scorpions has a statistically significant

242   adjusted R^2 value of 0.657 (p-value: 3.8e^{-04}; Figure 2). Furthermore, estimated muscle volume

243   has a significant correlation to the pinch force estimation (F-value: 29; p-value: 1.1e^{-04}). The

244   pterygotid muscle forces predicted from muscle cross-sectional area and muscle stress were

245   considerably higher than those based on the linear model (Supplemental Table 5).

246   The VM stress distributions for the examined scorpion chelae are categorised into three

247   main groups. The first group comprises *Androctonus amoreuxi*, *Caraboctonus keyserlingi*,

248   *Chactas* sp., *Hadogenes paucidens, Opistophthalmus boehmi*, and *Scorpio maurus*, each of

249   which exhibit relatively high VM stress across the entire model, with the highest VM stress

250   proximal to the articulation between the manus and moveable finger and along chelae (Figure

251   3A–F). These forms are typically stouter and have more pronounced proximal manus regions.

252   Notably, *Ca. keyserlingi*, *Ha. paucidens*, and *Sc. maurus* have higher stress along the movable

253   finger. The second group consists of *Androctonus australis*, *An. bicolor*, *Grophus flavopiceus*,

254   *Hadrurus arizonensis*, *Hottentotta gentili*, *Leiurus quinquestriatus*, and *Parabuthus*

255   *transvaalicus*. These models have overall lower VM stress in the manus and variable degrees of

256   VM stress along elongate chelae fingers (Figure 3G–M). *Androctonus australis, An. bicolor, Ha.*

257   *arizonensis*, *Le. quinquestriatus* and *Pa. traansvalicus* have high VM stress proximal to the

258   articulation between the manus and moveable finger, contrasting with *Gr. flavopiceus* and *Ho.*

259   *gentili* that have lower VM stress over the entire model. The third group contains *Bothriurus* sp.

260   and *Pandinoides cavimanus*. These models show low VM stress in the proximal manus section,

261   high VM stress at the articulation between the manus and moveable finger, and lower VM stress

262   along stout chelae (Figure 3N, P). Finally, *Opisthacanthus maculatus* is unique, with low VM

263   stress in the proximal manus region and higher VM stress along the chelae (Figure 3O). Overall,

264   these groupings are comparable to those presented by Van der Meijden et al. (2012a), where

265   chelae models were standardized for scale using force to surface area ratio.

266   Distributions of VM stress in the pterygotid models are broadly comparable to those of

267   scorpion FEMs (Figure 4). Although these appendages are not homologous—representing the

268   first and second limb-bearing segments in eurypterids and scorpions, respectively—the

269   functional analogy of the two can be tested with FEA. The observed VM stress similarity

270   strongly supports the idea that pterygotid chelicerae functioned like scorpion chelae indicating an

271   informative analogue for these fossil forms. Considering the mean VM stress distributions of the

272   scorpion and pterygotid models, the former have higher mean stress values (Figure 5). There is

273   limited clustering of family groups in bivariate space, reflecting the range of input force values

274   for the modelled scorpions (Supplemental Table 9). Taxa within the Buthidae in particular have a

275   large spread of stress within similar volume values. Within the pterygotids , the larger models

276   (*Jaekelopterus rhenaniae* and *Acutiramus bohemicus*) show the lowest mean stress.

277   Of the pterygotid models, *Erettopterus bilobus* and *Pterygotus anglicus* have comparable

278   VM stress along the fixed and free rami and proximal to the region of articulation between the

279   fixed and free rami (Figure 4A, B). *Pterygotus anglicus* shows high VM stress on the large

280   denticles and *Er. bilobus* has lower VM stress along the distal section of the free ramus.

281   *Jaekelopterus rhenaniae* has the lowest overall VM stress and its only high VM stress region is

282   proximal to the point of articulation between the fixed and free rami and along the proximal

283   section of the free ramus (Figure 4C). *Acutiramus bohemicus* has high VM stress in the region

284   proximal to the point of articulation between the fixed and free rami and along the proximal

285   section of the free ramus (Figure 4D). Further, the highest strain areas are located along the

286   oblique, serrated denticles.

287   In all FEMs, the VM stress is predictably concentrated in areas with high loads, such as

288   muscle insertions and around the fixed vertices on the denticles. In the scorpion models, higher

289   VM stress areas are visible on the proximal manus region – the location of simulated muscle

290   origins. However, scorpion chelae muscle origins are distributed across the majority of the

291   proximal manus region. As such, VM stress concentration on the proximal manus region reflect

292   where the models were constrained.

293   The large difference in estimated muscle force and stress distributions for the pterygotids

294   between the linear model and the cross-sectional area method is striking. As both methods are

295   commonly used, and both have weaknesses and assumptions, we opted to present the results of

296   both approaches to see if similar values could be predicted. The linear model predicted high

297   muscle force values for the pterygotids. However, as no extant chelicerates have comparably-

298   sized chelae or chelicerae, muscle forces were estimated by extrapolation rather than

299   interpolation. An unavoidable result of extrapolation is increased error. The cross-sectional area

300   method of muscle force estimation has more explicit assumptions, each with a level of

301   uncertainty. The range of lowest to highest muscle stress estimates illustrate this uncertainty

302   (Supplemental Table 5). For these reasons, we did not use the muscle force estimates derived

303   from cross-sectional area in the FEA models, and did not focus on absolute magnitudes of stress

304   or force in our analysis and discussion.

Discussion

306   The results of the scorpion FEA analysis show similar groupings as in Van der Meijden et al.

307   (2012a). The differences in magnitudes of VM stresses (Figure 3) indicate that some species (e.g.

308   *Pandinoides cavimanus, Ophistacanthus maculatus, Hottentotta gentili*) could exhibit a higher

309   'safety factor' (i.e., a measure of how much stronger a morphology needs to be compared to the

310   input forces; Hicks & Wang, 2021) than others (e.g. *Caraboctonus keyserlingi, Hadogenes*

311   *paucidens, Parabuthus transvaalicus*), although the pattern does not seem to correspond to

312   defensive behaviour (Van der Meijden et al., 2013) or relative pinch force (Simone & Van der

313   Meijden, 2018). Considering the modelled scorpions in the context of possible ecomorphs, there

314   is limited overlap between groups identified here and recently proposed ecomorphologies

315   (Coelho et al., 2022). This suggests that the FEMs produced here present more of an insight into

316   the effectiveness of these feeding tools, rather than inform on possible ecological groupings and

317   associated microhabitats. Combining these biomechanical analyses with detailed examination of

318   scorpion life modes will undoubtedly uncover new links between chelae mechanics and the diets

319   of these ecomorphs. However, this is beyond the scope of this work, as we have focused on using

320   scorpions to inform aspects of the pterygotid models. On this point, it is worth considering other

321   possible modern analogues for understanding and modelling pterygotids. Of particular note are

322   the camel spiders (Solifugae), which have large, dentate chelicerae that can grasp and

323   disarticulate prey for consumption (Van der Meijden et al., 2012b). These chelicerae are

324   anteriorly directed, but do not extend notably beyond the prosoma (Harms & Duperre, 2018).

325   While they may be informative for understanding how chelicerae can break prey, they are less

326   useful than scorpion pedipalps as functional analogues for prey capture by pterygotid chelicerae.

327   The morphology of pterygotid chelicerae suggests that these structures were used in

328   capturing prey for subsequent mastication by the coxal gnathobases (Waterston, 1964; Miller,

329   2007a). The solifuge comparisons made above suggest that the dentition of pterygotid chelicerae

330   may have allowed for some initial tearing of prey. This inferred feeding mode aligns with the co-

331   occurrence of pterygotids and proposed prey species, including other eurypterids, fishes, and a

332   likely array of soft-bodied animals that are not preserved(Rolfe, 1973; Chlupáč et al., 1980;

333   Kennedy et al., 2012). Furthermore, links between cheliceral and lateral compound eye

334   morphologies have been drawn to propose an apex predatory life mode for some pterygotids

335   (Anderson et al., 2014; McCoy et al., 2015).

336   Results of the FEA support previous inferences that pterygotid chelicerae, while having a

337   similar overall morphology, had differing functional capabilities (McCoy et al., 2015). The

338   comparable VM stress distributions between the chelicerae of *Erettopterus bilobus* and

339   *Pterygotus anglicus* suggest that these taxa would have experienced similar stresses during

340   predation and therefore probably targeted similar prey. Based on the known faunal assemblages

341   that co-occur with these pterygotid species (Dunlop et al., 2002; Miller, 2007b; Lebedev et al.,

342   2009; McCoy et al., 2015; Fyffe et al., 2016; Blieck, 2017; Supplemental Tables 10, 11), coupled

343   with the large body lengths of *Er. bilobus* (0.7 m) and *Pt. anglicus* (1.6 m), proposed prey

344   includes other eurypterids and fishes; in the case of the Devonian *Pt. anglicus*, the latter could

345   include armoured forms, such as ostracoderms and placoderms. This is further supported by the

346   moderate to high visual acuity in these pterygotid genera (McCoy et al., 2015), allowing them to

347   identify and pursue such mobile, possibly smaller prey. Indirect evidence for *Er. bilobus*

348   consuming fish comes in the form of coprolites rich in agnathan fragments from the

349   Lesmahagow Inlier, which have been previously attributed to eurypterid predation (Rolfe, 1973;

350   Selden, 1984). It therefore seems that *Er. bilobus* and *Pt. anglicus* were apex predators within

351   their respective ecosystems (Selden, 1984; Dunlop et al., 2002; Kennedy et al., 2012). This

352   seems to contradict the previous suggestions that *Er. bilobus* was a more generalised predator

353   than *Pt. anglicus* (McCoy et al., 2015).

354   The FEM of *Acutiramus bohemicus* produced a unique VM stress distribution associated

355   with its different cheliceral morphology. All *Acutiramus* species have elongate (some

356   hypertrophied), oblique, anteriorly-directed, serrated denticles (Chlupáč, 1994; Laub et al., 2010;

357   McCoy et al., 2015). High VM stress along the free rami and within the constrained denticles

358   suggest that *Acutiramus* was not well adapted to capture armoured or thick-shelled prey and may

359   have experienced failure when doing so (Laub et al., 2010). Indeed, *Acutiramus* does not co-

360   occur with a diverse fish fauna, but rather an array of other eurypterid taxa (Laub et al., 2010;

361   Anderson et al., 2014; Supplemental Table 12). The angled, serrated denticles would be more

362   consistent with piercing eurypterid cuticle (Laub et al., 2010; Anderson et al., 2014; Fyffe et al.,

363   2016) and the proximal denticles on the free ramus may have impaled prey (Laub et al., 2010).

364   After impaling, the prey would have been sliced by the serrated denticles as the chelicerae

365   closed. The serrations documented by Laub et al. (2010) are proximally orientated, suggesting

366   that after impaling, a victim would have had to tear itself from the serrations, likely causing more

367   damage. This conforms to the idea that *Acutiramus* was likely an ambush predator or scavenger

368   that fed on soft-bodied and lightly cuticularized taxa, based on its limited vision and cheliceral

369   morphology (Anderson et al., 2014; McCoy et al., 2015).

370   The *Jaekelopterus rhenaniae* model has overall low VM stress compared to the other

371   pterygotid models. These data, combined with a proposed 2.5 m body length (Braddy et al.,

372   2008), high visual acuity (McCoy et al., 2015; Poschmann et al., 2016), good swimming abilities

373   (Plotnick & Baumiller, 1988; Tetlie, 2007), and a diverse co-occurring fauna containing several

374   eurypterid and armoured fish species (Fyffe et al., 2016; Poschmann et al., 2016; Supplemental

375   Table 13), suggest that *Ja. rhenaniae* was capable of capturing large, highly mobile, armoured

376   prey. The robust chelicerae would have enabled the initial grabbing and manipulation of food

377   items, while the heavily sclerotised gnathobases on large coxae would have been employed in

378   prey mastication (including crushing of thick cuticle or biomineralised structures), comparable to

379   extant xiphosurids (Waterston, 1964; Botton, 1984; Poschmann et al., 2017; Bicknell et al.,

380   2018a, b). The large reinforced chelicerae, giant body size, and phylogenetically-derived position

381   of *Ja. rhenaniae* (Figure 6; Braddy et al., 2008) appear to represent a peak in pterygotid

382   cheliceral evolution that coincides with the rapid diversification of placoderms (Randle &

383   Sansom, 2019). As such, predatory Devonian eurypterids, epitomised by *Ja. rhenaniae*, likely

384   developed a toolkit to target armoured fish in the form of robust chelicerae for grabbing prey and

385   stout gnathobases for masticating said prey (Poschmann et al., 2017), as opposed to eurypterids

386   driving the radiation of placoderms (*contra* Romer, 1933). The extinction of pterygotids in the

387   Late Devonian is consistent with them ultimately being outcompeted by vertebrates (particularly

388   jawed fishes), cephalopods, and various other groups during the Devonian Nekton Revolution

389   (Lamsdell & Braddy, 2010; Klug et al., 2010, 2018), as well as falling victim to environmental

390   changes (Lamsdell & Selden, 2017).

391   **Conclusions**

392   Finite element models of chelicerae from four pterygotid eurypterids (*Acutiramus bohemicus*,

393   *Erettopterus bilobus*, *Jaekelopterus rhenaniae*, and *Pterygotus anglicus*) are presented and

394   compared with FEMs of modern scorpion chelae. Overall similarity in VM stress distribution

395   indicates that pterygotid chelicerae are functionally analogous to scorpion chelae, as suggested

396   by the morphological similarity of these structures. Considering the pterygotid VM stress

397   distributions in the context of their palaeoecology (including visual capabilities) and overall

398   cheliceral morphology, we have demonstrated, with FEA, the morpho-functional ability of these

399   ancient marine predators. We conclude that *Er. bilobus* and *Pt. anglicus* were apex predators

400   within their respective ecosystems and likely targeted other eurypterids and fishes. Stress

401   distributions of the *Ac. bohemicus* model, together with its unique denticle morphology, suggest

402 that the chelicera of this species was well adapted to piercing and slicing the cuticle of other

403 eurypterids. Finally, *Ja. rhenaniae*, the largest known pterygotid, experienced low VM stress

404 across the chelicera, suggesting that it was well adapted to capturing large, highly mobile,

405 armoured prey. These results demonstrate how 3D FEA can be applied across a range of

406 morphologies and used to explore the mechanical performance of extinct predatory arthropods.

407 **Data accessibility**

408 Scorpion pincer 3D PDFs, pterygotid chelicerae .STL models, and loaded FEA models can be

409 downloaded from 10.17605/OSF.IO/GV8J5.

410 **Author contributions**

411 R.D.C.B., J.R.P., G.D.E, A.v.d.M., and S.W. conceived the study. R.D.C.B., S.W., A.v.d.M., and

412 Y.S. collected and analysed the data. R.D.C.B., J.R.P., A.v.d.M., Y.S., and G.D.E. interpreted the

413 results, with input from the other authors. R.D.C.B. constructed figures. R.D.C.B. J.R.P.,

414 A.v.d.M., Y.S., and G.D.E. wrote the text. All authors discussed, edited and approved the

415 manuscript.

416 **Competing interests**

417 We declare we have no competing interests.

418 **Funding**

419 This research was supported by funding from an Australian Research Council Discovery Project

420 grant (DP200102005 to J.R.P., S.W., and G.D.E.), and a UNE Postdoctoral Research Fellowship

421 (to R.D.C.B). A.v.d.M. is financed through FCT, I.P. under contract number

422 DL57/2016/CP1440/CT0009. Y.S. was funded by a PhD scholarship by Fundação para Ciênciae

423 Tecnologia (SFRH/BD/136934/2018).

424 **Acknowledgements**

425 We thank Katrina Kenny for producing the 3D reconstructions of the fossil taxa, Thomas

426 Kleinteich for his help in scanning the scorpion chelae, and Jason Dunlop and Carolin Haug for

427 their constructive reviews.

428 **References**

429 **Anderson RP, McCoy VE, McNamara ME, Briggs DEG**. **2014**. What big eyes you have: the

430 ecological role of giant pterygotid eurypterids. *Biology Letters* **10 (7)**: 20140412.

431 **Attard MRG, Wilson LAB, Worthy TH, Scofield P, Johnston P, Parr WCH, Wroe S**. **2016**.

432 Moa diet fits the bill: virtual reconstruction incorporating mummified remains and

433 prediction of biomechanical performance in avian giants. *Proceedings of the Royal*

434 *Society of London B: Biological Sciences* **283 (1822)**: 20152043.

435 **Bicknell RDC, Ledogar JA, Wroe S, Gutzler BC, Watson III WH, Paterson JR**. **2018a**.

436 Computational biomechanical analyses demonstrate similar shell-crushing abilities in

437 modern and ancient arthropods. *Proceedings of the Royal Society of London B:*

438 *Biological Sciences* **285 (1889)**: 20181935.

439 **Bicknell RDC, Paterson JR, Caron J-B, Skovsted CB**. **2018b**. The gnathobasic spine

440 microstructure of Recent and Silurian chelicerates and the Cambrian artiopodan *Sidneyia*:

441 Functional and evolutionary implications. *Arthropod Structure & Development* **47 (1)**:

442 12–24.

443   **Bicknell RDC, Smith PM, Poschmann M**. **2020**. Re-evaluating evidence of Australian

444   eurypterids. *Gondwana Research* **86**: 164–181.

445   **Bicknell RDC, Holmes JD, Edgecombe GD, Losso SR, Ortega-Hernández J, Wroe S,**

446   **Paterson JR**. **2021**. Biomechanical analyses of Cambrian euarthropod limbs reveal their

447   effectiveness in mastication and durophagy. *Proceedings of the Royal Society of London*

448   *B: Biological Sciences* **288 (1943)**: 20202075.

449   **Blieck A**. **2017**. Heterostracan vertebrates and the Great Eodevonian Biodiversification Event—

450   an essay. *Palaeobiodiversity and Palaeoenvironments* **97 (3)**: 375–390.

451   **Botton ML**. **1984**. Diet and food preferences of the adult horseshoe crab *Limulus polyphemus* in

452   Delaware Bay, New Jersey, USA. *Marine Biology* **81 (2)**: 199–207.

453   **Braddy SJ, Poschmann M, Tetlie OE**. **2008**. Giant claw reveals the largest ever arthropod.

454   *Biology Letters* **4 (1)**: 106–109.

455   **Chlupáč I, Kříž J, Schönlaub HP, Klapper G, Zikmundová J**. **1980**. Silurian and Devonian

456   conodont localities of the Barrandian. *Second European Conodont Symposium (ECOS II),*

457   *Guidebook, Abstracts: Abhandlungen des Geologisches Bundesaltsalt.* p 147–180.

458   **Chlupáč I**. **1994**. Pterygotid eurypterids (Arthropoda, Chelicerata) in the Silurian and Devonian

459   of Bohemia. *Journal of the Czech Geological Society* **39 (2-3)**: 147–162.

460   **Cignoni P, Callieri M, Corsini M, Dellepiane M, Ganovelli F, Ranzuglia G**. **2008**. Meshlab:

461   an open-source mesh processing tool. *Sixth Eurographics Italian Chapter Conference:*

462   *Salerno, Italy.* p 129–136.

463   **Ciurca SJ, Tetlie OE**. **2007**. Pterygotids (Chelicerata; Eurypterida) from the Silurian Vernon

464   Formation of New York. *Journal of Paleontology* **81 (4)**: 725–736.

465   **Coelho P, Kaliontzopoulou A, Sousa P, Stockmann M, van der Meijden A**. **2022**.

466   Reevaluating scorpion ecomorphs using a naïve approach. *BMC Ecology and Evolution*

467   **22 (1)**: 17.

468   **Dalingwater JE**. **1973**. The cuticle of a eurypterid. *Lethaia* **6 (2)**: 179–185.

469   **Dalingwater JE**. **1975**. Further observations on eurypterid cuticles. *Fossils and Strata* **4**: 271–

470   279.

471   **Dalingwater JE**. **1985**. Biomechanical approaches to eurypterid cuticles and chelicerate

472   exoskeletons. *Transactions of the Royal Society of Edinburgh: Earth Sciences* **76 (2-3)**:

473   359–364.

474   **Dumont ER, Grosse IR, Slater GJ**. **2009**. Requirements for comparing the performance of

475   finite element models of biological structures. *Journal of Theoretical Biology* **256 (1)**:

476   96–103.

477   **Dunlop JA, Braddy SJ, Tetlie E**. **2002**. The Early Devonian eurypterid *Grossopterus overathi*

478   (Gross, 1933) from Overath, Germany. *Mitteilungen aus dem Museum für Naturkunde in*

479   *Berlin Geowissenschaftliche Reihe* **5 (1)**: 93–104.

480   **Dunlop JA, Penney D, Jekel D**. **2020**. A summary list of fossil spiders and their relatives.

481   *World Spider Catalog, version 20.5*: Natural History Museum Bern.

482   **Esteve J, Marcé-Nogué J, Pérez-Peris F, Rayfield E**. **2021**. Cephalic biomechanics underpins

483   the evolutionary success of trilobites. *Palaeontology* **64 (4)**: 519–530.

484   **Fyffe L, Johnson S, van Staal C**. **2016**. A review of Proterozoic to Early Paleozoic lithotectonic

485   terranes in the northeastern Appalachian orogen of New Brunswick, Canada, and their

486   tectonic evolution during Penobscot, Taconic, Salinic, and Acadian orogenesis. *Atlantic*

487   *Geology* **47**: 211–248.

488   **Gilai A, Parnas I**. **1970**. Neuromuscular physiology of the closer muscles in the pedipalp of the

489   scorpion *Leiurus quinquestriatus*. *Journal of Experimental Biology* **52 (2)**: 325–344.

490   **Harms D, Duperre N**. **2018**. An annotated type catalogue of the camel spiders (Arachnida:

491   Solifugae) held in the Zoological Museum Hamburg. *Zootaxa* **4375 (1)**: 1–58.

492   **Haug C**. **2020**. The evolution of feeding within Euchelicerata: data from the fossil groups

493   Eurypterida and Trigonotarbida illustrate possible evolutionary pathways. *PeerJ* **8**:

494   e9696.

495   **Hicks JW, Wang T**. **2021**. Safety factors as a 'design' principle of animal form and function: an

496   historical perspective. *Journal of Experimental Biology* **224 (22)**: jeb243324.

497   **Kellersztein I, Cohen SR, Bar-On B, Wagner HD**. **2019**. The exoskeleton of scorpions'

498   pincers: Structure and micro-mechanical properties. *Acta Biomaterialia* **94**: 565–573.

499   **Kennedy KL, Miller RF, Gibling MR**. **2012**. Palaeoenvironments of Early Devonian fish and

500   other aquatic fauna of the Campbellton Formation, New Brunswick, Canada.

501   *Palaeogeography, Palaeoclimatology, Palaeoecology* **361**: 61–72.

502   **Kjellesvig-Waering EN**. **1964**. A synopsis of the family Pterygotidae Clarke and Ruedemann,

503   1912 (Eurypterida). *Journal of Paleontology* **38 (2)**: 331–361.

504   **Klug C, Kroeger B, Kiessling W, Mullins GL, Servais T, Frýda J, Korn D, Turner S**. **2010**.

505   The Devonian nekton revolution. *Lethaia* **43 (4)**: 465–477.

506   **Klug C, Frey L, Pohle A, De Baets K, Korn D**. **2018**. Palaeozoic evolution of animal

507   mouthparts. *Bulletin of Geosciences* **92 (4)**: 511–524.

508   **Kupczik K, Dobson CA, Crompton RH, Phillips R, Oxnard CE, Fagan MJ, O'Higgins P**.

509   **2009**. Masticatory loading and bone adaptation in the supraorbital torus of developing

510   macaques. *American Journal of Physical Anthropology* **139 (2)**: 193–203.

511 **Lamsdell JC, Braddy SJ**. **2010**. Cope's Rule and Romer's theory: patterns of diversity and

512   gigantism in eurypterids and Palaeozoic vertebrates. *Biology Letters* **6 (2)**: 265–269.

513 **Lamsdell JC, Selden PA**. **2017**. From success to persistence: identifying an evolutionary regime

514   shift in the diverse Paleozoic aquatic arthropod group Eurypterida, driven by the

515   Devonian biotic crisis. *Evolution* **71 (1)**: 95–110.

516 **Laub RS, Tollerton VP, Berkof RS**. **2010**. The cheliceral claw of *Acutiramus* (Arthropoda:

517   Eurypterida): functional analysis based on morphology and engineering principles.

518   *Bulletin of the Buffalo Society of Natural Sciences* **39**: 29–42.

519 **Lebedev OA, Mark-Kurik E, Karatajūtė-Talimaa VN, Lukševičs E, Ivanov A**. **2009**. Bite

520   marks as evidence of predation in early vertebrates. *Acta Zoologica* **90**: 344–356.

521 **Legg DA, Sutton MD, Edgecombe GD**. **2013**. Arthropod fossil data increase congruence of

522   morphological and molecular phylogenies. *Nature Communications* **4**: 2485.

523 **Lomax DR, Lamsdell JC, Ciurca SJ**. **2011**. A collection of eurypterids from the Silurian of

524   Lesmahagow collected pre 1900. *Geological Curator* **9 (6)**: 331–348.

525 **Lourenço WR**. **2021**. Scorpion diversity and distribution: Past and present patterns. In:

526   Gopalakrishnakone P, ed. *Toxinology: Scorpion Venoms*. Dordrecht: Springer

527   Netherlands, 1–20.

528 **McCoy VE, Lamsdell JC, Poschmann M, Anderson RP, Briggs DEG**. **2015**. All the better to

529   see you with: eyes and claws reveal the evolution of divergent ecological roles in giant

530   pterygotid eurypterids. *Biology Letters* **11 (8)**: 20150564.

531 **Miller RF**. **2007a**. Nineteenth century collections of *Pterygotus anglicus* Agassiz (Chelicerata;

532   Eurypterida) from the Campbellton Formation, New Brunswick, Canada. *Atlantic*

533   *Geology* **43**: 197–209.

534 **Miller RF**. **2007b**. *Pterygotus anglicus* Agassiz (Chelicerata: Eurypterida) from Atholville,

535   Lower Devonian Campbellton Formation, New Brunswick, Canada. *Palaeontology* **50**

536   **(4)**: 981–999.

537 **Plotnick RE, Baumiller TK**. **1988**. The pterygotid telson as a biological rudder. *Lethaia* **21 (1)**:

538   13–27.

539 **Poschmann M, Franke C**. **2006**. Arthropods and trace fossils from the Lower Devonian

540   (Emsian) of the West Eifel region/Germany and the Grand Duchy of Luxembourg.

541   *Ferrantia* **46**: 97–115.

542 **Poschmann M, Tetlie OE**. **2006**. On the Emsian (Lower Devonian) arthropods of the Rhenish

543   Slate Mountains: 5. Rare and poorly known eurypterids from Willwerath, Germany.

544   *Paläontologische Zeitschrift* **80 (4)**: 325–343.

545 **Poschmann M, Schoenemann B, McCoy VE**. **2016**. Telltale eyes: the lateral visual systems of

546   Rhenish Lower Devonian eurypterids (Arthropoda, Chelicerata) and their

547   palaeobiological implications. *Palaeontology* **59 (2)**: 295–304.

548 **Poschmann M, Bergmann A, Kühl G**. **2017**. First record of eurypterids (Chelicerata,

549   Eurypterida) from the Lower Devonian (Lower Emsian) Hunsrück Slate (SW Germany).

550   *PalZ* **91 (2)**: 163–169.

551 **R Development Core Team**. **2021**. R: a language and environment for statistical computing.

552   4.1.2 ed. *Vienna, Austria: R Foundation for Statistical Computing*.

553 **Randle E, Sansom RS**. **2019**. Bite marks and predation of fossil jawless fish during the rise of

554   jawed vertebrates. *Proceedings of the Royal Society B* **286 (1917)**: 20191596.

555 **Rayfield EJ, Norman DB, Horner CC, Horner JR, Smith PM, Thomason JJ, Upchurch P**.

556   **2001**. Cranial design and function in a large theropod dinosaur. *Nature* **409 (6823)**:

557   1033–1037.

558 **Rayfield EJ**. **2007**. Finite element analysis and understanding the biomechanics and evolution of

559   living and fossil organisms. *Annual Reviews in Earth and Planetary Sciences* **35**: 541–

560   576.

561 **Rolfe WDI**. **1973**. Excursion 15: Silurian arthropod and fish assemblages from Lesmahagow,

562   Lanarkshire. In: Bluck BJ, ed. *Excursion guide to the geology of the Glasgow District*.

563   Glasgow: Geological Society of Glasgow, 119–126.

564 **Romer AS**. **1933**. Eurypterid influence on vertebrate history. *Science* **78 (2015)**: 114–117.

565 **Ross CF**. **2005**. Finite element analysis in vertebrate biomechanics. *The Anatomical Record Part*

566   *A* **283 (2)**: 253–258.

567 **Rowe AJ, Snively E**. **2022**. Biomechanics of juvenile tyrannosaurid mandibles and their

568   implications for bite force: Evolutionary biology. *The Anatomical Record* **305 (2)**: 373–

569   392.

570 **Selden PA**. **1984**. Autecology of Silurian eurypterids. *Special Papers in Palaeontology* **32**: 39–

571   54.

572 **Shultz JW**. **2007**. A phylogenetic analysis of the arachnid orders based on morphological

573   characters. *Zoological Journal of the Linnean Society* **150**: 221–265.

574 **Simone Y, Van der Meijden A**. **2018**. Fast and fine versus strong and stout: a trade-off between

575   chela closing force and speed across nine scorpion species. *Biological Journal of the*

576   *Linnean Society* **123 (1)**: 208–217.

577 **Snodgrass RE**. **1952**. A Textbook of Arthropod Anatomy. Cornell University Press, Ithaca.

578   **Stahnke HL**. **1970**. Scorpion nomenclature and mensuration. *Entomological News* **81 (12)**: 297–

579   316.

580   **Størmer L**. **1936**. Eurypteriden aus dem rheinischen Unterdevon. *Abhandlungen der*

581   *Preußischen Geologischen Landesanstalt* **175**: 1–74.

582   **Strait DS, Weber GW, Neubauer S, Chalk J, Richmond BG, Lucas PW, Spencer MA,**

583   **Schrein C, Dechow PC, Ross CF**. **2009**. The feeding biomechanics and dietary ecology

584   of *Australopithecus africanus*. *Proceedings of the National Academy of Sciences* **106 (7)**:

585   2124–2129.

586   **Tetlie OE**. **2007**. Distribution and dispersal history of Eurypterida (Chelicerata).

587   *Palaeogeography, Palaeoclimatology, Palaeoecology* **252 (3-4)**: 557–574.

588   **Van der Meijden A, Herrel A, Summers A**. **2010**. Comparison of chela size and pincer force in

589   scorpions; getting a first grip. *Journal of Zoology* **280 (4)**: 319–325.

590   **Van der Meijden A, Kleinteich T, Coelho P**. **2012a**. Packing a pinch: functional implications

591   of chela shapes in scorpions using finite element analysis. *Journal of Anatomy* **220 (5)**:

592   423–434.

593   **Van der Meijden A, Langer F, Boistel R, Vagovic P, Heethoff M**. **2012b**. Functional

594   morphology and bite performance of raptorial chelicerae of camel spiders (Solifugae).

595   *Journal of Experimental Biology* **215 (19)**: 3411–3418.

596   **Van der Meijden A, Lobo Coelho P, Sousa P, Herrel A**. **2013**. Choose your weapon:

597   defensive behavior is associated with morphology and performance in scorpions. *PLoS*

598   *ONE* **8 (11)**: e78955.

599   **van Heteren AH, Wroe S, Tsang LR, Mitchell DR, Ross P, Ledogar JA, Attard MRG,**

600   **Sustaita D, Clausen P, Scofield RP**. **2021**. New Zealand's extinct giant raptor

601   (*Hieraaetus moorei*) killed like an eagle, ate like a condor. *Proceedings of the Royal*

602   *Society B: Biological Sciences* **288 (1964)**: 20211913.

603   **Vermeij GJ**. **2016**. Gigantism and its implications for the history of life. *PLoS ONE* **11 (1)**:

604   e0146092.

605   **Waterston CD**. **1964**. Observations on pterygotid eurypterids. *Transactions of the Royal Society*

606   *of Edinburgh* **66 (2)**: 9–33.

607   **Wroe S, McHenry C, Thomason J**. **2005**. Bite club: comparative bite force in big biting

608   mammals and the prediction of predatory behaviour in fossil taxa. *Proceedings of the*

609   *Royal Society of London B: Biological Sciences* **272 (1563)**: 619–625.

610   **Wroe S, Clausen P, McHenry C, Moreno K, Cunningham E**. **2007**. Computer simulation of

611   feeding behaviour in the thylacine and dingo as a novel test for convergence and niche

612   overlap. *Proceedings of the Royal Society B: Biological Sciences* **274 (1627)**: 2819–2828.

613   **Wroe S, Parr WCH, Ledogar JA, Bourke J, Evans SP, Fiorenza L, Benazzi S, Hublin J-J,**

614   **Stringer C, Kullmer O, Curry M, Rae TC, Yokley TR**. **2018**. Computer simulations

615   show that Neanderthal facial morphology represents adaptation to cold and high energy

616   demands, but not heavy biting. *Proceedings of the Royal Society of London B: Biological*

617   *Sciences* **285 (1876)**: 20180085.

618

619

Figure captions

620

621 **Figure 1:** Theoretical models used for the biomechanical analyses, colour coded for analogous

622 structures. (A) Scorpion model. (B) Pterygotid model. Abbreviation: h, hinge. Muscle fibre

623 organisation is used to illustrate generalised muscle directions but was not used to determine

624 muscle force (see Methods).

625 **Figure 2:** 3D scatterplot of the relationship between scorpion pinch force and muscle volume

626 and surface. The grey section represents the correlation across the three variables.

627 **Figure 3**: Lateral views of scorpion finite element models showing von Mises (VM) brick stress

628 maps. (A): *Androctonus amoreuxi* Sc450. (B): *Caraboctonus keyserlingi* Sc3009. (C):

629 *Opistophthalmus boehmi* Sc696. (D): *Chactas* sp. Sc999. (E): *Hadogenes paucidens* Sc1041. (F):

630 *Scorpio maurus* Sc1. (G): *Androctonus australis* Sc707 (H): *Parabuthus transvaalicus* Sc 2. (I)

631 *Androctonus bicolor* Sc2623. (J): *Grophus flavopiceus* Sc881. (K): *Hottentotta gentili* Sc172.

632 (L): *Leiurus quinquestriatus* Sc1062. (M): *Hadrurus arizonensis* Sc1004. (N): *Bothriurus* sp.

633 Sc675. (O): *Opisthacanthus maculatus* Sc877. (P): *Pandinoides cavimanus* Sc761. (B, E, F, H, J,

634 K, O) mirrored to align with other appendages. Biomechanical models are found in

635 Supplemental Data 1–16.

636 **Figure 4:** Lateral views of solved finite element models of assessed pterygotids showing von

637 Mises (VM) brick stress maps. (A): *Erettopterus bilobus* from the Silurian (latest Llandovery and

638 Wenlock) Patrick and Kip Burn formations, Scotland. (B): *Pterygotus anglicus* from the

639 Devonian (Emsian) Campbellton Formation, Canada. (C): *Jaekelopterus rhenaniae* from the

640 Devonian (Emsian) Klerf and Nellenköpfchen formations, Germany. (D): *Acutiramus bohemicus*

641   from the Silurian (Pridoli) Požáry Formation, Czech Republic. Biomechanical models are found

642   in Supplemental Data 17–20.

643

644   **Figure 5:** Scatterplot of the relationship between log transformed VM stress and log transformed

645   model volume for scorpions and pterygotids.

646   **Figure 6:** Simplified phylogeny of analysed pterygotid taxa showing total body lengths (in

647   metres), associated time ranges and FEMs. Derived from Braddy et al. (2008; fig. 2) and

648   Lamsdell & Selden (2017; fig. 1).

649

650   **Supplemental Figure 1:** Lateral views of solved *Erettopterus bilobus* FEMs, exploring the

651   impact of modelled cuticle thickness and use of cross-sectional area to predict input force.

652   Overall similarity in stress distributions illustrates how cuticle thickness has limited impact on

653   the model. The majority of the variation occurs proximal to the hinge. The use of cross-sectional

654   area to predict muscles produces higher stress, but the distribution is comparable to the model in

655   Figure 3. (A): *Erettopterus bilobus* model in Figure 3. (B): *Erettopterus bilobus* with constrained

656   hollow denticles. (C): *Erettopterus bilobus* with thicker fixed and free ramus cuticle. (D):

657   *Erettopterus bilobus* with thinner fixed and free ramus cuticle. (E): *Erettopterus bilobus* model in

658   Figure 3 using input force derived from cross-sectional area. The stress is higher than Figure 3,

659   but the distribution is consistent. Biomechanical models are found in Supplemental Data 17.

660

661   **Supplemental Data 1**: 3D PDF and loaded Strand7 model for *Androctonus amoreuxi.*

662   **Supplemental Data 2**: 3D PDF and loaded Strand7 model for *Caraboctonus keyserlingi.*

663   **Supplemental Data 3**: 3D PDF and loaded Strand7 model for *Opistophthalmus boehmi.*

664   **Supplemental Data 4**: 3D PDF and loaded Strand7 model for *Chactas* sp.

665   **Supplemental Data 5**: 3D PDF and loaded Strand7 model for *Hadogenes paucidens*.

666   **Supplemental Data 6**: 3D PDF and loaded Strand7 model for *Scorpio maurus*.

667   **Supplemental Data 7**: 3D PDF and loaded Strand7 model for *Androctonus australis*.

668   **Supplemental Data 8**: 3D PDF and loaded Strand7 model for *Parabuthus transvaalicus.*

669   **Supplemental Data 9**: 3D PDF and loaded Strand7 model for *Androctonus bicolor*.

670   **Supplemental Data 10**: 3D PDF and loaded Strand7 model for *Grophus flavopiceus*.

671   **Supplemental Data 11**: 3D PDF and loaded Strand7 model for *Hottentotta gentili.*

672   **Supplemental Data 12**: 3D PDF and loaded Strand7 model for *Leiurus quinquestriatus.*

673   **Supplemental Data 13**: 3D PDF and loaded Strand7 model for *Hadrurus arizonensis.*

674   **Supplemental Data 14**: 3D PDF and loaded Strand7 model for *Bothriurus* sp.

675   **Supplemental Data 15**: 3D PDF and loaded Strand7 model for *Opisthacanthus maculatus*.

676   **Supplemental Data 16**: 3D PDF and loaded Strand7 model for *Pandinoides cavimanus*.

677   **Supplemental Data 17**: 3D reconstructions as .STLs and loaded Strand7 model for *Erettopterus*

678   *bilobus*, including sensitivity analyses.

679 **Supplemental Data 18**: 3D reconstructions as .STLs and loaded Strand7 model for *Pterygotus*

680 *anglicus*.

681 **Supplemental Data 19**: 3D reconstructions as .STLs and loaded Strand7 model for

682 *Jaekelopterus rhenaniae*.

683 **Supplemental Data 20**: 3D reconstructions as .STLs and loaded Strand7 model for *Acutiramus*

684 *bohemicus*.

685

686   **Supplemental Table 1:** Dataset used to estimate pinch force of the scanned specimens.

687   **Supplemental Table 2:** Regression coefficients of the species-specific models.

688   **Supplemental Table 3:** Dataset used to calculate muscle force at insertion.

689   **Supplemental Table 4**: Summary of specimens that were used to reconstruct the pterygotid
690   chelicerae for analysis.

691   **Supplemental Table 5:** Lower and upper values of input force for pterygotids as predicted by
692   cross-sectional area.

693   **Supplemental Table 6**: Summary of the linear model.

694   **Supplemental Table 7**: ANOVA results of the linear model.

695   **Supplemental Table 8**: Muscle volume, muscle surface, and input force estimation of
696   eurypterids.

697   **Supplemental Table 9:** Mean VM stress and model volumes.

698   **Supplemental Table 10**: Faunal list of the Lower Devonian (Emsian) Campbellton Formation,
699   Canada. Modelled species in bold. Data derived from Shear et al. (1996), Wilson (2006),
700   Kennedy et al. (2012), Miller et al. (2012), Fyffe et al. (2016), and Burrow et al. (2017).

701   **Supplemental Table 11:** Faunal list of the Silurian (latest Llandovery and Wenlock) Patrick and
702   Kip Burn formations, Scotland. Modelled species in bold. Data derived from Jones & Woodward
703   (1885), Rolfe & Fritz (1966), Howells (1982), Boucot & Janis (1983), Briggs & Clarkson
704   (1987), Märss & Ritchie (1997), Anderson (1999), Tetlie & Braddy (2003), Tetlie & Poschmann
705   (2008), and Perrier et al. (2019).

706   **Supplementary Table 12**: Faunal list of the Silurian (Pridoli) Požáry Formation, Czech

707   Republic. Modelled species in bold. Data derived from Chlupáč et al. (1980), Kříž et al. (1986),

708   Kříž (1992), Chlupáč (1994), Mergl (2001, 2019), Horný (2004, 2005), Südkamp & Burrow

709   (2007), Manda & Turek (2009), Manda & Frýda (2010), and Budil et al. (2014).

710   **Supplemental Table 13**: Faunal list of the Lower Devonian (Emsian) Klerf and Nellenköpfchen

711   formations, Germany. Modelled species in bold. Data derived from Fürsich & Hurst (1980),

712   Dunlop & Poschmann (1997), Anderson et al. (1998), Wehrmann et al. (2005); Poschmann

713   (2006), Poschmann & Franke (2006), Poschmann & Tetlie (2006), Braddy et al. (2008),

714   Poschmann et al. (2017), Schultze & Cumbaa (2017), Müller et al. (2018), Van Viersen &

715   Taghon (2020), and Mondéjar-Fernández et al. (2021).

716   **Supplemental Code 1**: R code used in regression analyses.

Figure 1

Figure 1: Theoretical models used for the biomechanical analyses, colour coded for analogous structures.

(A) Scorpion model. (B) Pterygotid model. Abbreviation: h, hinge. Muscle fibre organisation is used to illustrate generalised muscle directions but was not used to determine muscle force (see Methods).
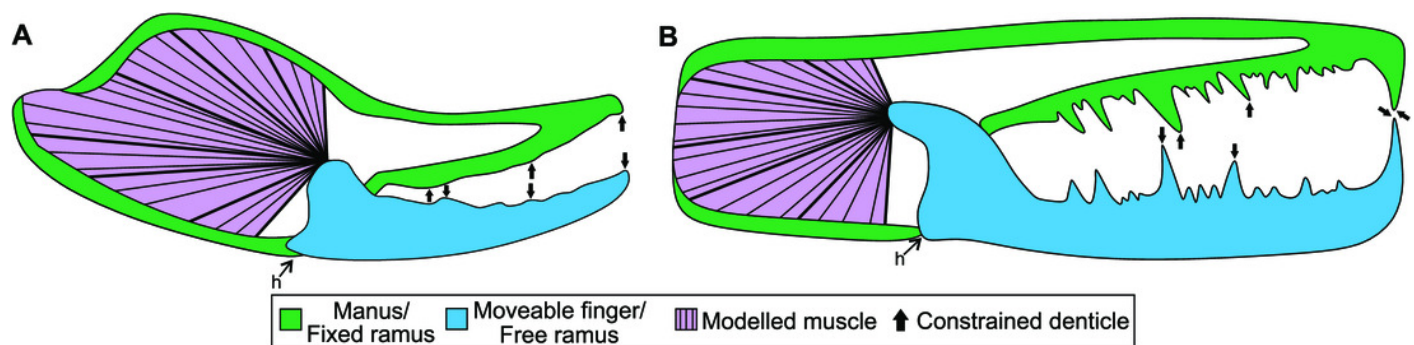
Figure 2

Figure 2: 3D scatterplot of the relationship between scorpion pinch force and muscle volume and surface.

The grey section represents the correlation across the three variables.
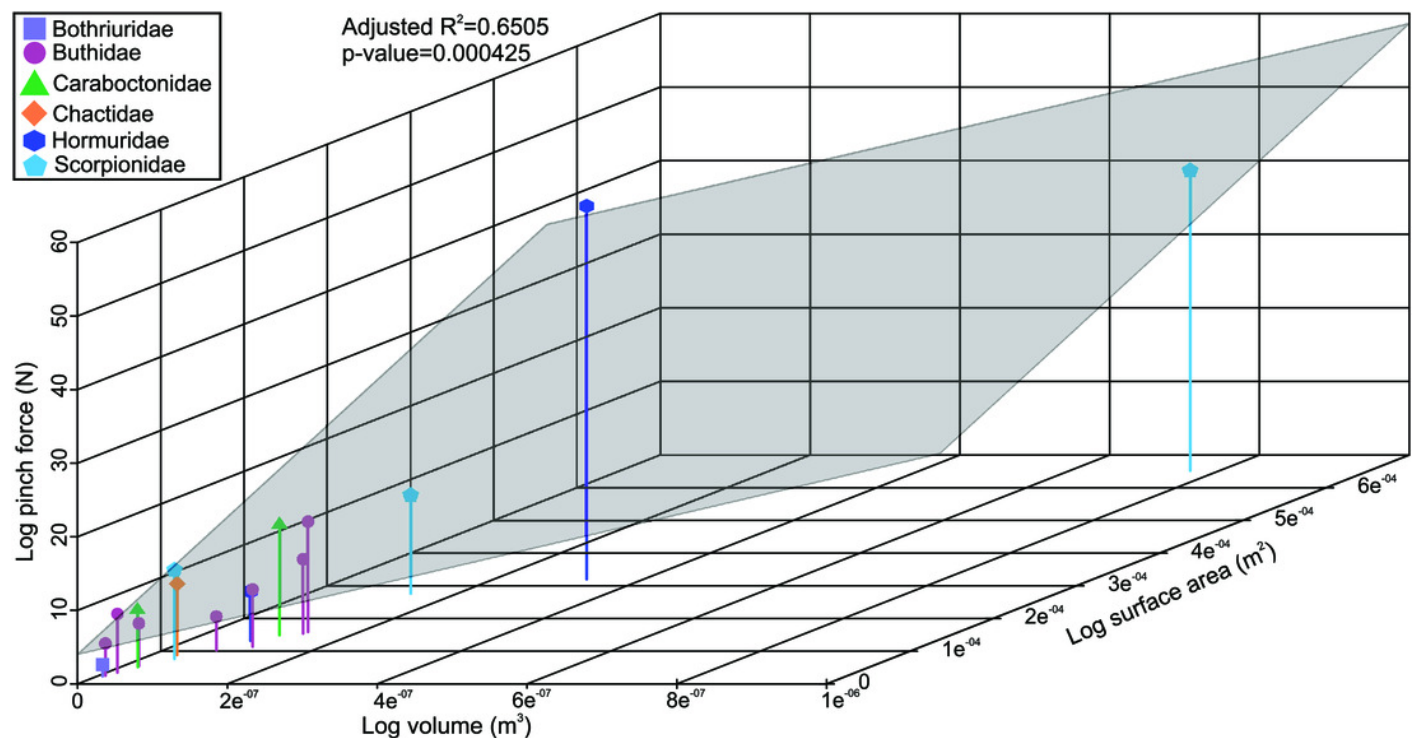
Figure 3

Figure 3: Lateral views of scorpion finite element models showing von Mises (VM) brick stress maps.

(A): *Androctonus amoreuxi* Sc450. (B): *Caraboctonus keyserlingi* Sc3009. (C): *Opistophthalmus boehmi* Sc696. (D): *Chactas* sp. Sc999. (E): *Hadogenes paucidens* Sc1041. (F): *Scorpio maurus* Sc1. (G): *Androctonus australis* Sc707 (H): *Parabuthus transvaalicus* Sc 2. (I) *Androctonus bicolor* Sc2623. (J): *Grophus flavopiceus* Sc881. (K): *Hottentotta gentili* Sc172. (L): *Leiurus quinquestriatus* Sc1062. (M): *Hadrurus arizonensis* Sc1004. (N): *Bothriurus* sp. Sc675. (O): *Opisthacanthus maculatus* Sc877. (P): *Pandinoides cavimanus* Sc761. (B, E, F, H, J, K, O) mirrored to align with other appendages. Biomechanical models are found in Supplemental Data 1–16.
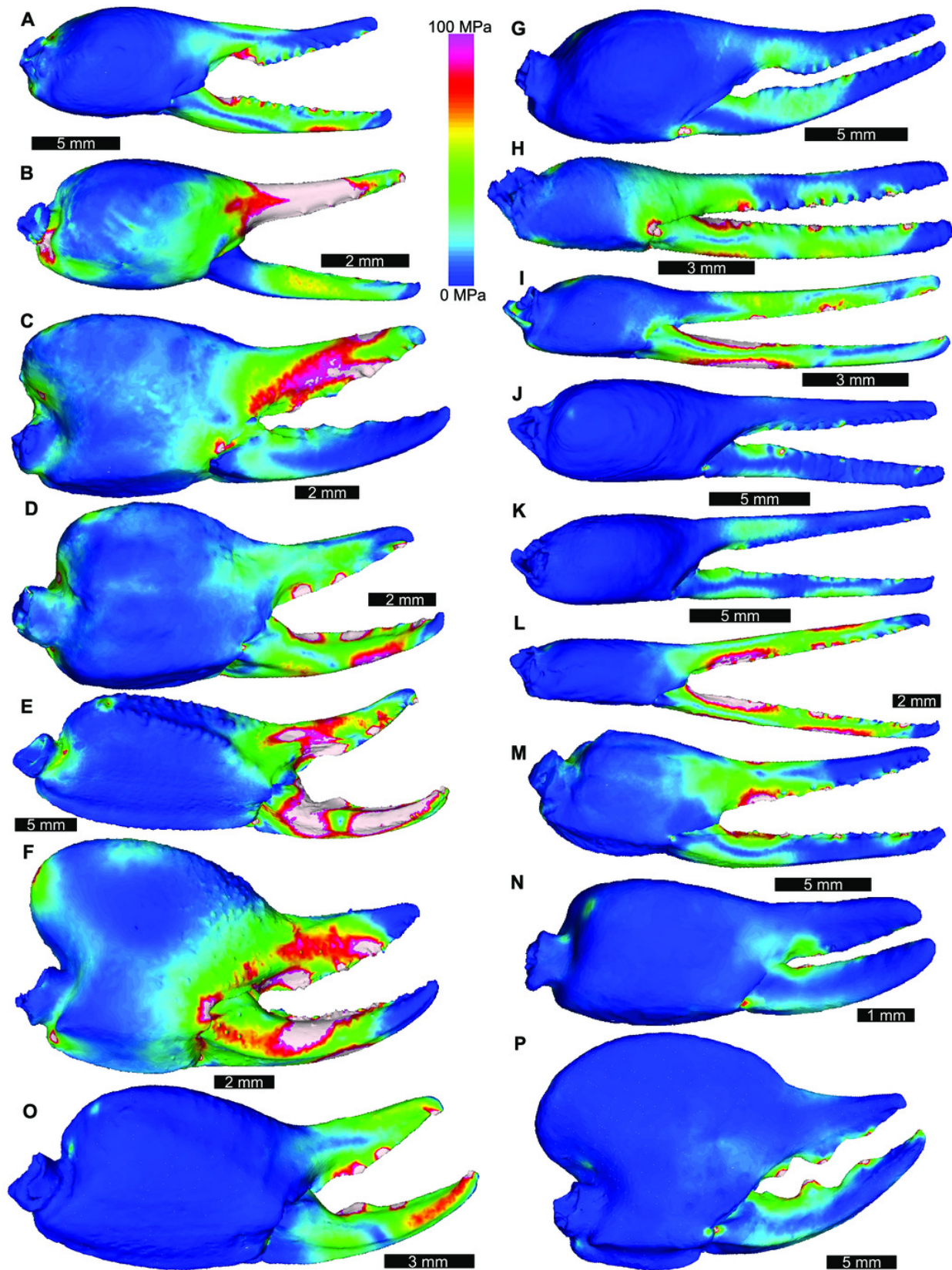
Figure 4

Figure 4: Lateral views of solved finite element models of assessed pterygotids showing von Mises (VM) brick stress maps.

(A): *Erettopterus bilobus* from the Silurian (latest Llandovery and Wenlock) Patrick and Kip Burn formations, Scotland. (B): *Pterygotus anglicus* from the Devonian (Emsian) Campbellton Formation, Canada. (C): *Jaekelopterus rhenaniae* from the Devonian (Emsian) Klerf and Nellenköpfchen formations, Germany. (D): *Acutiramus bohemicus* from the Silurian (Pridoli) Požáry Formation, Czech Republic. Biomechanical models are found in Supplemental Data 17–20.

A

10 mm

B

10 mm

100 MPa

0 MPa

C

50 mm

D

20 mm
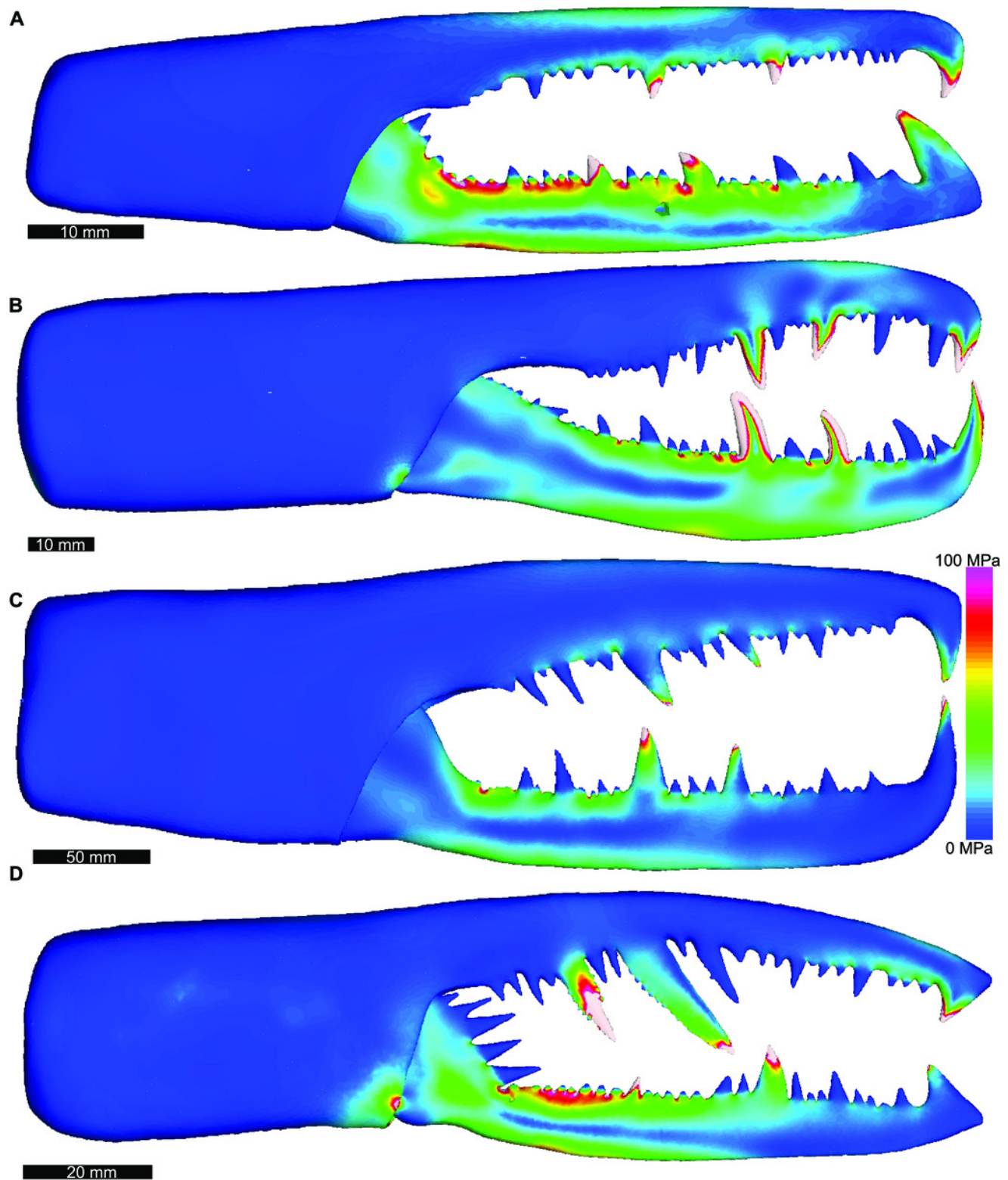
Figure 5

Figure 5: Scatterplot of the relationship between log transformed VM stress and log transformed model volume for scorpions and pterygotids.
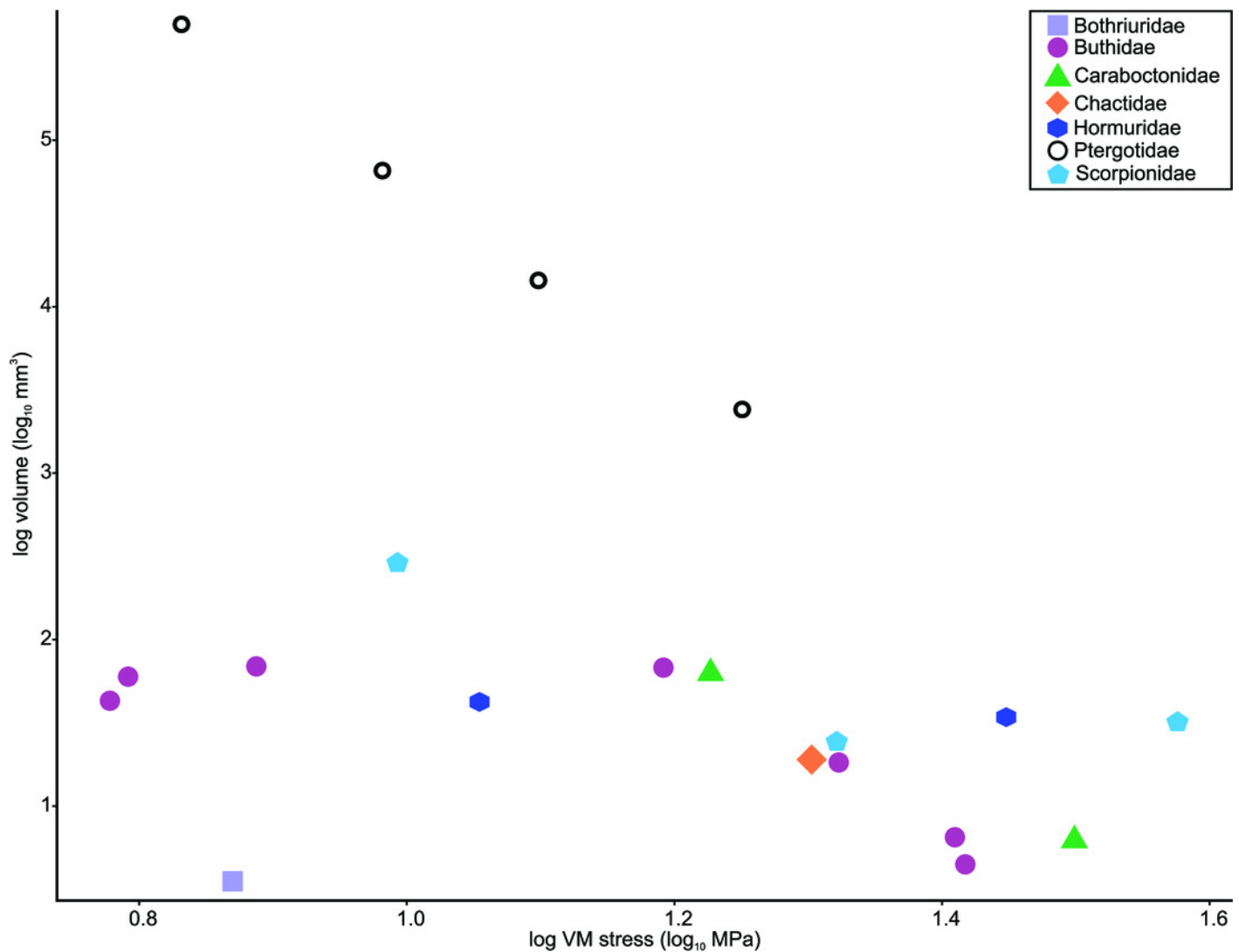
Figure 6

Figure 6: Simplified phylogeny of analysed pterygotid taxa showing total body lengths (in metres), associated time ranges and FEMs.

Derived from Braddy et al. (2008; fig. 2) and Lamsdell & Selden (2017; fig. 1).